Phys. Med. Biol. **43** (1998) 3065–3081. Printed in the UK PII: S0031-9155(98)92429-0

Optical properties of bovine muscle tissue *in vitro*; a comparison of methods

Jaap R Zijp and Jaap J ten Bosch

Materia Technica, Faculty of Medical Sciences, Bloemsingel 10, 9712 KZ Groningen, The Netherlands

Received 12 March 1998, in final form 1 July 1998

Abstract. We measured the optical properties of muscular tissue using several methods. Collimated transmission measurements of thin slabs showed spatial anisotropy of the scattering processes. Surface roughness of the sample disables the calculation of the extinction coefficient from these measurements. From angular intensity measurements we found a scattering asymmetry parameter $g = 0.96$. In fresh samples the optical diffusion constant D depends on the orientation with respect to the longitudinal direction of the muscular cells. From the D values we calculated s' perpendicular to the longitudinal direction as 0.19 mm^{-1} (at 543 nm), 0.39 mm^{-1} (at 594 nm) and 0.59 mm^{-1} (at 632 nm). The values for D which we measured from samples that were frozen and thawed did not show dependence on orientation. From spectral dependent reflectance measurements we found an oxygenation degree of 0.61 and a reduced scattering coefficient $s' = 0.85$ mm^{-1} around 560 nm.

1. Introduction

During the last few decades a huge increase in the use of optical methods for medical applications has occurred. Not only has the number of clinical measurements increased, but a wide variety of methods has also been developed. Examples are found in very different fields of interest like arterial blood oxygenation measurement, dental caries quantification, and cancer treatment with photodynamic therapy. Many of these methods use light in the visible and near-infrared wavelength range. In the case of determination of tissue conditions, light with an appropriate wavelength is sent into the tissue, scattered and partially absorbed. Scattered light is detected in various geometries.

Researchers involved in meat and science industry have developed optical meat quality assessment methods. Using these methods meat is classified in three quality groups, without using the single scattering and absorption properties (Davis *et al* 1978, Birth *et al* 1978).

We are interested in the development of new methods for the detection of optical properties of tissues deeper in the human body. In that case not only the skin but also muscular tissue has to be passed by the used light. Optimization of signal detection requires knowledge of the optical properties, like absorption and scattering coefficients and the scattering asymmetry parameter, of this muscular tissue. Properties previously obtained by several authors are given in table 1. A significant gap in this information is the wavelength dependence of these optical properties, which is why we performed the presented measurements.

0031-9155/98/103065+17$19.50

Table 1. Values of optical properties of mammalian muscular tissue as published by several authors.

Wavelength (nm)	Species	Absorption coefficient (mm^{-1})	Scattering coefficient (mm^{-1})	Asymmetry parameter	Author
630	Pig	0.082	4.1	0.824	Wilksch *et al* (1983)
633	Bovine			0.954 ± 0.016	Flock *et al* (1987)
515	Human	11.2 ± 1.8	530 ± 44	—	Marchesini *et al* (1989)
630	Rabbit	0.14 ± 0.02	11 ± 0.5	0.846 ± 0.009	Beek *et al* (1997)
630	Pig	0.12 ± 0.01	23.9 ± 1.6	0.732 ± 0.013	Beek *et al* (1997)
633	Rabbit	0.074 ± 0.006	14.0 ± 0.6	0.968 ± 0.002	Beek *et al* (1997)
633	Pig	0.059 ± 0.001	17.9 ± 1.2	0.858 ± 0.012	Beek *et al* (1997)
790	Rabbit	0.23 ± 0.02	15.7 ± 1.1	0.950 ± 0.005	Beek *et al* (1997)

2. Estimates of scattering and absorption parameters

Whole muscle contains cells which have the form of a fibre, their diameter is typically 25 μm (Rhodin 1975). They are oriented in the longitudinal direction of the muscle. Between these cells are capillary blood vessels, with widths ranging from 4 to 6 μm; they are oriented parallel and across the longitudinal direction. Their number is nearly equal to the number of muscle cells. At some places larger blood vessels (55 μm width), nerves, periaxial spaces (containing neuromuscular spindles and intrafusal muscle fibres) and lymphatic vessels are present. Within the muscular cells the mitochondria and nuclei can be seen. All these structures will contribute to light scattering and absorption, because their refractive indices are different from their surroundings. The irregular forms and different sizes of the structures make it impossible to predict the absorption and scattering coefficients exactly.

The spatial anisotropy of muscular tissue results in anisotropy of the scattering process. We expect that the scattering coefficient s parallel to the longitudinal direction is minimal with respect to that in all other directions, as the fibre-like cells can be considered as cylinders whose scattering cross section is vanishing at incidence parallel to the cylinder axes. Because of the presence of small structures, we expect that scattering coefficient decreases as the wavelength of light increases. We expect that the value of s perpendicular to the longitudinal direction is of the order of the reciprocal size of the cells, i.e. 40 mm^{-1}.

The angular intensity function $i(\theta)$, which describes the single scattered intensity as a function of the scattering angle θ, will be peaked in the forward direction (around $\theta = 0^\circ$) due to the large structures, but also a wide backscattering peak (around $\theta = 180^\circ$) may be expected from the presence of small structures.

The scattering asymmetry parameter g is defined as the mean value of $\cos\theta$. For scattering structures very small compared with the wavelength λ $g = 0$, and $g \simeq 1$ for large structures. The wavelength dependence of g of the tissue will be a result of two competing processes. Firstly, for small particles the scattering cross section is proportional to $1/\lambda^4$, so an increase of the wavelength will cause a decrease of the contribution due to small particles and so an increase of g. Secondly the scattering cross section of large structures is about constant as the wavelength increases. Their g values are not simple functions of the wavelength, but they show a general tendency to decrease as the wavelength increases. Because the first process is a fourth-order process we expect that g will increase with increasing wavelength.

The main light absorbers in muscles are myoglobin and the haemoglobin present in the red blood cells in the blood vessels. The absorption spectra of myoglobin and haemoglobin

are nearly equal. Figure 1 shows the absorption spectra of oxy- and deoxymyoglobin. These substances play a role in oxygen transport within the tissue. From the iron content, which is known to be 23 mg kg^{-1} (Souci *et al* 1969) we can calculate the myoglobin content as 0.41 mmol kg^{-1}. Muscle tissue, as we used it, contained a remnant blood concentration of about 3 vol.%; from this value and the iron content of bovine blood, which is 490 mg kg^{-1} (Souci *et al* 1969), we calculated the haemoglobin content as 0.066 mmol kg^{-1}.

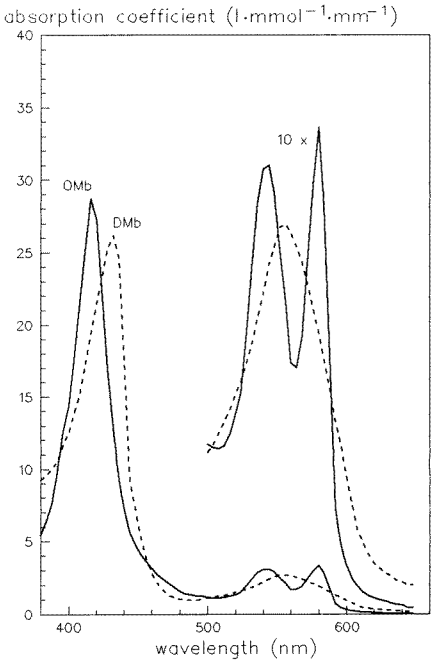

Figure 1. Absorption spectra of oxy- and deoxymyoglobin, obtained by decadic coefficients from the literature (Antonini and Brunori 1971), multiplied with ln(10) and 0.1 (cm mm^{-1}). Multiplication of the shown values by the concentration in mmol l^{-1} gives the naperian values of the linear absorption coefficients in mm^{-1}.

In the following calculations we will consider absorption due to myoglobin only, because its concentration is much higher than the haemoglobin concentration. From the myoglobin content and the values read from figure 1 we can estimate the absorption coefficient a to be in the order of 0.4–1.5 mm^{-1} at wavelengths ranging from 500 to 600 nm.

In living tissues myoglobin and haemoglobin are present in their oxygenated and deoxygenated forms, while *post mortem* the concentrations of their deoxygenated forms are higher, because the metabolism of the cells continues, while the oxygen supply is stopped. At a cut surface, which is exposed to air, the degree of oxygenation will be higher than is valid for the whole sample.

2.1. Transmission of thin slabs

The spatial anisotropy of the tissue will cause anisotropy in the scattering process. More light will be scattered perpendicularly to the longitudinal direction than parallel to this direction. This phenomenon can be observed by transmission through thin slabs.

The attenuation coefficient, which is equal to the sum of the scattering and absorption coefficients, can be determined by measuring the collimated transmission of a light beam by optically thin slabs of tissue. By application of Beer's law we can calculate

$$\mu = (s + a) = \frac{-\ln(T_c)}{d}$$

with μ the attenuation coefficient in mm^{-1}, s the scattering coefficient in mm^{-1}, a the absorption coefficient in mm^{-1}, T_c the collimated transmission and d the thickness in mm.

2.2. The angular intensity function $i(\theta)$ and the asymmetry parameter g

For measurement of the angular intensity function we used the set-up shown in figure 2. A Xe arclamp as a light source is combined with a monochromator, the exit port of which is focused upon the sample. The measured scattered light has to be considered as the convolution of the single scattering angular intensity function of the slab and the angular intensity distribution of the incident beam. We define

$$h(\theta) = \int_{\theta'=0^\circ}^{180^\circ} \mathrm{d}\theta'\, i(\theta')\, j(\theta - \theta') \tag{1}$$

with θ the scattering angle, h the measured angular intensity distribution, i the single scattering angular intensity function of the slab, j the angular intensity distribution of the incident beam.

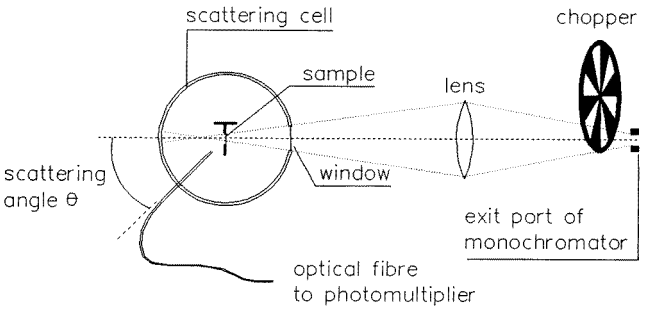

Figure 2. Set-up as used for the measurement of the wavelength-dependent scattering angular intensity functions.

Finding $i(\theta)$ by deconvolution is not feasible because the measured $h_{\text{meas}}(\theta)$ has a limited number of points and cannot be measured at large angles. A convenient way to find $i(\theta)$ is to fit the calculated function $h_{\text{calc}}(\theta)$ to the measured angular distribution $h_{\text{meas}}(\theta)$. The function $h_{\text{calc}}(\theta)$ is calculated by equation (1) as a convolution of the unscattered beam $j(\theta)$ and an estimated function $i_{\text{calc}}(\theta)$. As an approximation for $i_{\text{calc}}(\theta)$ a linear combination of two Henyey–Greenstein functions ($P_{\text{H–G}}$) can be used (Marchesini *et al* 1989):

$$i_{\text{calc}}(\theta) = bP_{\text{H–G}}(g_1) + (1 - b)P_{\text{H–G}}(g_2)$$

with

$$P_{\text{H–G}}(g) = \frac{1 - g^2}{(1 + g^2 - 2g\cos\theta)^{3/2}}.$$

By adjusting g_1, g_2 and b the best fitting $i_{\text{calc}}(\theta)$ can be found, and is considered as the single scattering angular intensity function.

The asymmetry parameter g_{fit}, i.e. the mean cosine of the scattering angle, for the scattering process by thin slabs can be calculated by:

$$g_{\text{fit}} = \frac{\int_{\theta=0^\circ}^{180^\circ} \mathrm{d}\theta\, i_{\text{calc}}(\theta) \sin\theta \cos\theta}{\int_{\theta=0^\circ}^{180^\circ} \mathrm{d}\theta\, i_{\text{calc}}(\theta) \sin\theta}.$$

If the thickness of the slabs is smaller than the mean free path of the photons, we are dealing with single scattering, and so g_{fit} determined in this way will not depend on the slab thickness. As we pointed out earlier, we expect that g_{fit} is increasing with increasing wavelength.

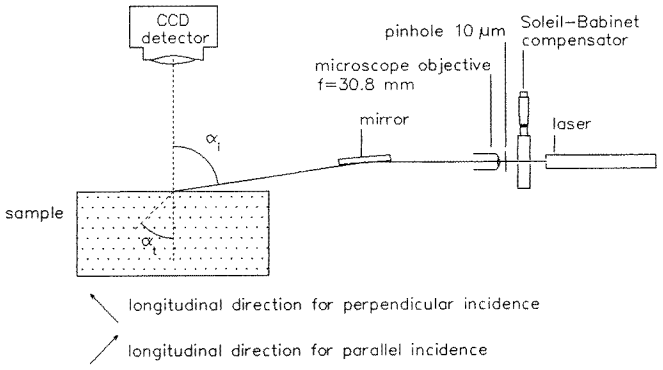

Figure 3. Set-up as used for the measurement of the diffusion constant D.

2.3. The diffusion constant D

Lin *et al* (1997) presented an easy method for determining the diffusion constant D, with the measurement geometry as shown in figure 3. A laser beam is obliquely incident on the top face of a scattering and absorbing sample. From the top of this sample a reflectance pattern can be observed. This pattern is imaged on a two-dimensional CCD detector. The incident beam can be observed as the most intense area in the image. At distances $\gg D$ from this spot the reflectance pattern is circularly symmetric. From the distance between the centre of this circle and the centre of the incident laser beam the diffusion constant can be calculated as

$$D = \frac{\Delta x\, n_{\text{tissue}}}{3 \sin\alpha_i} \tag{2}$$

with D the diffusion constant in mm, Δx the distance in mm, n_{tissue} the refractive index of the sample and α_i the angle of incidence of the laser beam with respect to the normal of the outer surface.

According to Lin *et al* (1997) this diffusion constant is equal to

$$D = \frac{1}{3(0.35a + s')}$$

with s' the reduced scattering coefficient, i.e. $s(1 - g)$.

2.4. Spectral dependence of reflectance

The difference in the absorption spectra of oxy- and deoxymyoglobin offers the opportunity to determine the degree of oxygenation of an optically thick tissue slab from measurement of the diffuse reflectance spectrum.

When an infinitely thick slab of scattering and absorbing material is diffusely illuminated, Kubelka–Munk theory may be applied to calculate the ratio of Kubelka–Munk scattering and absorption coefficients, K/S, from the diffuse reflectance (Judd and Wyszecki 1963)

$$\left(\frac{K}{S}\right)_{\text{meas}}(\lambda) = \frac{(R_\infty(\lambda)-1)^2}{2R_\infty(\lambda)} \tag{3}$$

with K the absorption coefficient for diffuse light, i.e. $K = 2a$ in mm^{-1} (Meador and Weaver 1979), S the scattering coefficient for diffuse light, $S = \frac{1}{4}(3s' - a)$ in mm^{-1} (Meador and Weaver 1979) and R_∞ the measured diffuse reflectance, ∞ indicating an infinitely thick scattering and absorbing layer.

Kubelka–Munk theory assumes refractive index matching between the outside medium (air) and the sample. The corrections that we performed are explained in the materials and methods section. Assuming an oxidation degree and a scattering contribution the function $(K/S)_{\text{calc}}(\lambda)$ can be calculated and fit to the measured values $(K/S)_{\text{meas}}(\lambda)$. We calculate $(K/S)_{\text{calc}}(\lambda)$ by

$$\left(\frac{K}{S}\right)_{\text{calc}}(\lambda) = \frac{8a(\lambda)}{3b_2 - a(\lambda)}$$

with

$$a(\lambda) = b_1\, a_{\text{OMb}}(\lambda) + (1-b_1)\, a_{\text{OMb}}(\lambda)$$

with $a_{\text{OMb}}(\lambda)$ as the absorption coefficient (in mm^{-1}) of oxymyoglobin, $a_{\text{DMb}}(\lambda)$ as the absorption coefficient (in mm^{-1}) of deoxymyoglobin, and b_1 and b_2 as the fitting parameters. Note that $a_{\text{OMb}}(\lambda)$ and $a_{\text{DMb}}(\lambda)$ are calculated from the myoglobin concentration and the values shown in figure 1. After fitting, b_1 is equal to the degree of oxygenation of the myoglobin and b_2 equals the reduced scattering coefficient s' in mm^{-1}, which we assume to be independent of the wavelength within the used wavelength range of 530–586 nm.

3. Materials and methods

3.1. Samples

All experiments were carried out on samples cut from bovine *psoas major* muscles, fetched from the butcher less than three days after slaughter. After boning the samples were vacuum packed, these packs were opened just before measurement.

Samples used for collimated transmission measurements and angular intensity function measurements were prepared from tissue blocks with a volume of about 1 cm^3, which were frozen with carbon dioxide snow. From these blocks slabs with thicknesses of 14, 20, 30, 35, 40 and 55 μm were cut with a microtome. These samples were kept frozen at $-22\,^\circ$C until measurement. Before measurement the slabs were put between two microscope coverslips in order to keep them flat. Two kinds of tissue were distinguished, the slabs containing muscular cells and slabs cut from the white connective tissue, which unites muscle cells into bundles.

Samples used for the spectral reflectance measurements were kept unfrozen and measured instantly after unpacking. Their typical dimensions were a diameter of 70 mm and a thickness of 20 mm. These samples and samples which were frozen and thawed were used for the determination of the diffusion constant.

3.2. Transmission of thin slabs

With the set-up as shown in figure 4 we measured the transmission of the tissue slabs. With two microscope coverslips at the sample holder, the 25 μm pinhole was imaged at the CCD camera by use of a microscope objective. We used an area of 100×100 pixels of the CCD camera, which was placed at 800 mm distance from the sample holder. One pixel in distance on the camera represented an observation angle of 2.9×10^{-5} rad with respect to the sample. This image was interpreted as collimated transmission $T_c = 1.0$. The two coverslips were removed from the sample holder and exchanged with a sample between two coverslips. Removal and replacement of the cuvette caused a move of the position of the most intense illuminated pixels. Therefore we used the CCD camera pixels within circles of radii of 2 and 5 pixel distances around the pixel containing the highest value for the transmission calculations. The collimated transmission of each slab was measured at the same wavelengths as those used with the angular intensity function measurements.

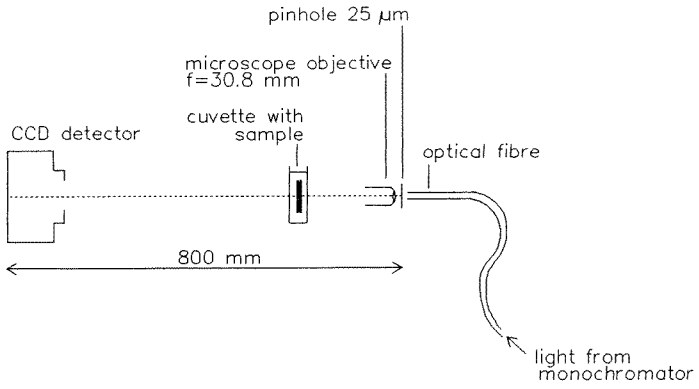

Figure 4. Set-up as used for the collimated transmission measurements of thin tissue slabs.

3.3. The angular intensity function $i(\theta)$ and asymmetry parameter g

The samples were placed in the scattering cell, filled with saline to prevent osmotic effects and to minimize refraction at the surfaces. The longitudinal cells were oriented perpendicular to the scattering plane during these measurements. Our set-up, as shown in figure 2, was comparable with the one used by Jacques *et al* (1987). However, we used a high-pressure Xe arclamp with a monochromator as a light source. The output port of the monochromator, which had a diameter of 4 mm, was focused upon the sample. Measurements were performed at wavelengths 550, 600, 633, 667, 700, 733, 767, 800 and 833 nm. At wavelengths longer than 633 nm an additional red filter was used, in order to cut off wavelengths shorter than 600 nm, which passed the monochromator as second-order maxima.

The scattered light was collected by an optical fibre mounted in a rotatable bracket, hanging in the saline. This collecting fibre covered a solid angle of 2.8×10^{-4} sr with respect to the centre of the sample. A photomultiplier (Hamamatsu R5600-01), whose spectral response extends from 280–830 nm, was used as a detector. By applying a chopper in the incident beam, and lock-in amplification, optimal signal detection was obtained. The scattered light could be measured at angles ranging from 0° to 167°. The scattering angle was measured with a resolution of 0.25°. With the same set-up the angular intensity function of the incident beam $j(\theta)$ was measured.

3.4. Determination of the diffusion constant D

The experimental set-up that we used to measure D is shown in figure 3. A laser beam from a tunable HeNe laser (4.0 mW at 632.8 nm, 0.5 mW at 594.1 nm and 0.3 mW at 543.5 nm; Electro-Optics, model LSTPC-1010) is incident on a Soleil–Babinet compensator (Melles Griot 04 SBC 001). The compensator is adjusted so that the linearly polarized light from the laser is converted to circularly polarized light with a remnant linear polarized component smaller than 1%, at the three wavelengths used. This light was incident on a pinhole. This pinhole was imaged in the plane coincident with the top surface of the sample, using a microscope objective (Melles Griot 04 OAS 006), creating an elliptical incident beam of 175 μm $\times$ 1.25 mm. We could not use the entire laser beam as the incident beam because this method demands an incident beam of the same size or smaller than the diffuse reflection pattern at the top surface of the sample. The index of refraction of bovine muscular tissue is about 1.40 at 630 nm (Bolin *et al* 1989). In order to create an incident angle of 45° within the sample we had to apply the incident beam at an incident angle of 82° outside the sample. The top surfaces of the samples were cut at 45° with respect to the longitudinal direction of the muscular cells. The samples were placed at two different orientations (being perpendicular and parallel) to the longitudinal direction with respect to the (inner) incident beam, as indicated in by the arrows in figure 3.

The reflection pattern was imaged on a two-dimensional CCD detector (EG&G Parr 1433C) using an enlarger lens (Rodenstock, Apo-Rodagon, 80 mm F/4-F/22). Empirically we found that imaging an area of about 10×10 mm of the top surface of the sample at 300×300 pixels of the CCD camera lead to reliable results. The images from the CCD camera were shown, as false colour pictures (different colours representing different intensities), on a computer monitor screen. On this screen a small circular cursor (corresponding to 0.2 mm on the sample) was put 'by hand' at the centre of the image of the laser beam. A large circle (4 mm at the sample) was manipulated so that it was concentric with the diffuse reflectance pattern. The horizontal distance between the centre of the cursor and the centre of the large circle was used as Δx in equation (2).

3.5. Spectral reflectance measurements

We measured the reflectance of the sample with the geometry shown in figure 5. The light source was a blue-coated incandescent lamp (Philips daylight blue 100 W), made for photographic applications. Its spectrum compares better with illuminant A than with normal daylight D65. A spectroradiometer (Photoresearch PR-650) was used as a detector, it supplies the reflectance spectrum from 380 to 780 nm, in steps of 4 nm. The reflectance spectrum R'_∞ of the sample was obtained as the ratio of the measured spectrum of the

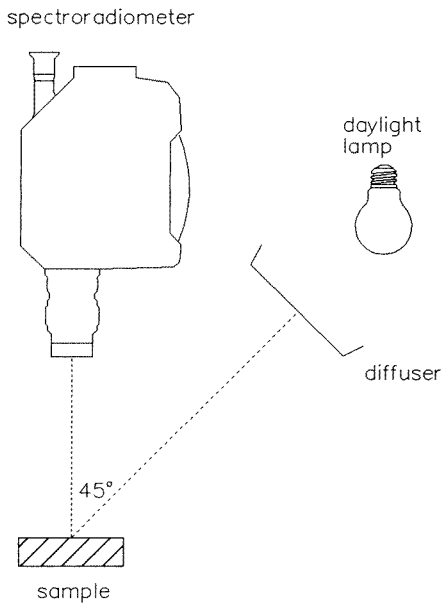

Figure 5. Set-up as used for the measurement of the spectral reflectance.

sample and the measured spectrum of a white standard, in order to account for the spectral distribution of the light source. We used a spectralon block (Labsphere, Spectralon SRM-99O) as a white standard, having a reflectance $R_\infty(\lambda) > 0.98$ over this wavelength range. Note that fluorescence is neglected when this method is used.

The applied Kubelka–Munk theory assumes refractive index matching between the outside medium (air) and the sample. We have to perform two corrections to account for the refractive index step at the air–tissue boundary. Firstly, less light will enter the medium than in the refractive index matching case. Secondly, the observed reflectance is lower than in the case of refractive index matching, due to internal reflection of light present within the sample at the boundary. An expression performing both these corrections is given by Molenaar *et al* (in preparation). In short: the light entering the medium is attenuated by a factor $1-r_{45^\circ}$; the light emerging from the medium is attenuated by a factor $1-r_i$, and multiple reflections between boundary and medium are represented by a series $1+R_\infty r_i + R_\infty^2 r_i^2 + \cdots = 1/(1-R_\infty r_i)$. This leads to

$$R_\infty(\lambda) = \frac{R'_\infty(\lambda)}{(1-r_{45^\circ})(1-r_i) + R'_\infty(\lambda) r_i} \tag{4}$$

with

$$r_{45^\circ} = \frac{\tan^2(\theta_i - \theta_t)}{2\tan^2(\theta_i + \theta_t)} + \frac{\sin^2(\theta_i - \theta_t)}{2\sin^2(\theta_i + \theta_t)}$$

$$\theta_t = \arcsin\left(\frac{\sin\theta_i}{n}\right)$$

and

$$r_i = 1 - \frac{1 - r_e}{n^2}$$

$$r_e = \frac{1}{2} + \frac{(n-1)(3n+1)}{6(n+1)^2} + \frac{n^2(n^2-1)^2}{(n^2+1)^3} \ln\left(\frac{n-1}{n+1}\right) - \frac{2n^3(n^2+2n-1)}{(n^2+1)(n^4-1)} + \frac{8n^4(n^4+1)}{(n^2+1)(n^4-1)^2} \ln(n)$$

with R_∞ the reflectance of an infinitely thick sample with a refractive index matched with the outside medium (air), R'_∞ the reflectance of an infinitely thick sample with a refractive index different from the outside medium, θ_i the angle of incidence, i.e. 45° in our case, and n the refractive index of the sample, $n = 1.40$ for muscular tissue (Bolin *et al* 1989). r_i and r_e are the surface reflection coefficients for diffuse illumination from internal and external respectively, the formula for r_e is given by Duntley (1942). The values calculated by equation (4) were used in equation (3) to obtain $(K/S)_{\text{meas}}(\lambda)$.

4. Results

4.1. Transmission of thin slabs

The transmitted intensity distributions from muscular cell samples, as imaged on the CCD, were not circular symmetric; an example is shown in figure 6. From such intensity patterns obtained with three 14 μm thick samples we measured the long and short axes of the contour representing 0.1× the maximum measured value, and determined its long-axis to short-axis ratio. The results are given in table 2. The intensity distributions as transmitted by the connective tissue were circularly symmetric.

From the measured collimated transmissions we calculated the extinction coefficients μ for both the muscular cell samples and the connective tissue samples, the obtained values are also given in table 2.

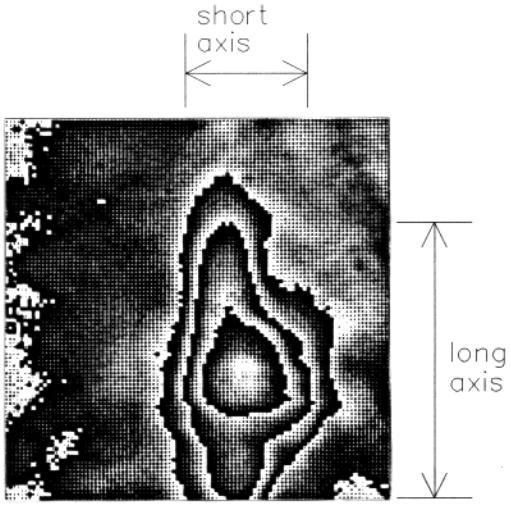

Figure 6. Example of the intensity pattern transmitted by a 14 μm thick sample of muscular tissue. One contrast gradient series from white to black represents a decrease of intensity with a factor $\sqrt{10}$.

Table 2. Results of the transmission measurements: mean values with standard errors of the mean (SEM) of ratios of long- and short-axes of the patterns, and values of μ (mm^{-1}).

	Wavelength (nm)								
	550	600	633	667	700	733	767	800	833
Muscular cell samples									
Mean ratio	2.27	2.40	2.72	2.66	2.72	2.88	2.82	3.07	3.09
SEM	0.13	0.20	0.30	0.23	0.11	0.33	0.35	0.53	0.41
Mean μ[a]	139	136	136	136	147	124	134	128	125
SEM (mm^{-1})	13	15	17	19	20	23	22	21	20
Connective tissue samples									
Mean μ[a]	137	128	140	137	129	133	132	132	127
SEM (mm^{-1})	9	9	10	9	9	10	11	11	10

[a] These values are too high, see text for explanation.

4.2. Angular intensity function $i(\theta)$ and asymmetry parameter g

The incident beam had a full width at half maximum of about 3°. A total of 188 measured angular intensity functions of muscular cell slabs, and 262 of connective tissue, were measured and analysed. Examples of the functions $h_{meas}(\theta)$, $h_{calc}(\theta)$ and $i_{calc}(\theta)$ are shown in figure 7. The minimum in $h_{meas}(\theta)$ around 90° is caused by the shade of the sample holder.

Analysis of the results of the muscular cell samples showed the following mean and SEM values, $g_1 = 0.976 \pm 0.001$, $g_2 = -0.243 \pm 0.019$, $b = 0.985 \pm 0.001$ and $g_{fit} = 0.961 \pm 0.001$, averaged over all thicknesses and wavelengths. Multiple regression analysis from the statistical package SPSS/PC+ (SPSS Inc.) showed that these values were not dependent on the sample thickness. The wavelength dependence of the g_{fit} values is shown in figure 8.

The results obtained from the connective tissue samples showed $g_{fit} = 0.841 \pm 0.006$, averaged over all wavelengths and sample thicknesses. With multiple regression analysis we found that g_{fit} depends on the sample thickness.

4.3. Diffusion constant D

Table 3 shows the mean and SEM values of D ($n = 9$, three samples, three measurements at each sample for each wavelength) calculated by equation (2) with Δx measured from three fresh and three frozen and thawed samples. Analysis of the CCD images showed us that at 543 nm, where considerable absorption takes place, more than 75% of the detected light is multiple scattered.

4.4. Spectral reflectance measurements

The mean value of eight spectral reflectance measurements $R'_\infty(\lambda)$ and its standard deviation are shown in figure 9. Examples of the obtained K/S are shown in figure 10. After the fitting procedure we found an oxygenation degree of $b_1 = 0.61 \pm 0.01$ and a reduced scattering coefficient $b_2 = s' = 0.85 \pm 0.04$ mm^{-1}.

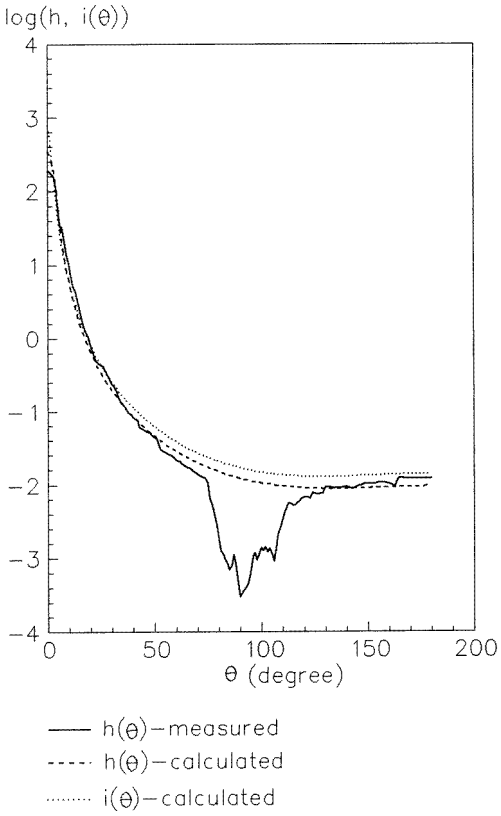

Figure 7. Examples of measured and calculated angular intensity functions. $h_{\mathrm{meas}}(\theta)$ is directly measured, $h_{\mathrm{calc}}(\theta)$ is fit to this function using a convolution of an estimated single scattering angular intensity function $i(\theta)$ with the unscattered beam $j(\theta)$.

5. Discussion

5.1. Transmission of the slabs

From table 2 we see that the forward scattering pattern elongates as the wavelength increases. This can be explained in the following way. At short wavelengths the contribution of small particles to the scattering process is larger than at longer wavelengths. These small particles, like structures within the cells, are randomly oriented and will on average scatter circularly symmetrically with respect to the forward direction. At higher wavelengths scattering by larger structures, being the oblong cells, becomes relatively more important. Due to their orientation more light will be scattered in directions nearly perpendicular to the longitudinal direction, as can be observed.

Table 2 also shows that the extinction coefficients for the muscular cell samples and connective tissue samples decrease with increasing wavelength. As the absorption coefficient is much smaller than the scattering coefficient it is reasonable that this effect is due to a decrease of the latter. So this behaviour can also be explained by a diminishing contribution of small structures. The values will be discussed in section 5.5.

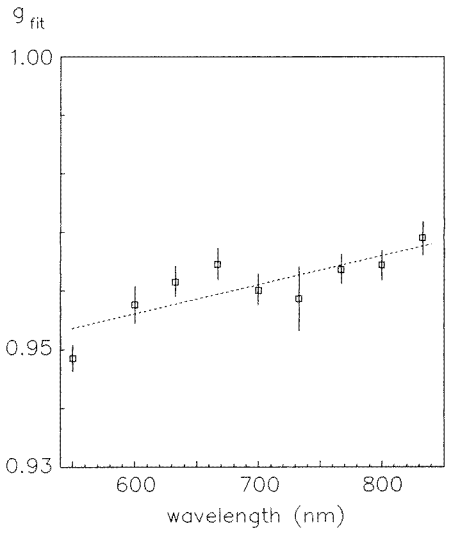

Figure 8. Wavelength dependence of the g_{fit} values found for muscular cell samples.

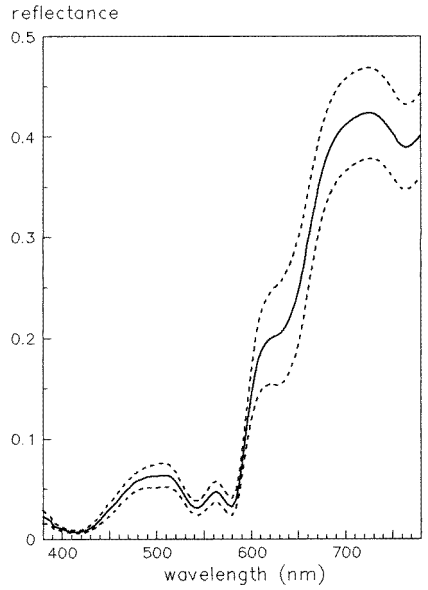

Figure 9. Mean values and standard deviations of eight spectral reflectance measurements $R'_{\infty}(\lambda)$ of a thick slab of muscular tissue.

5.2. Angular intensity functions

For the muscular cell samples we found that the values g_1, g_2, b and g_{fit} did not depend on the sample thickness. This indicates that the samples are thin enough to cause single scattering. The increase in the values found for g_{fit} with increasing wavelength can be

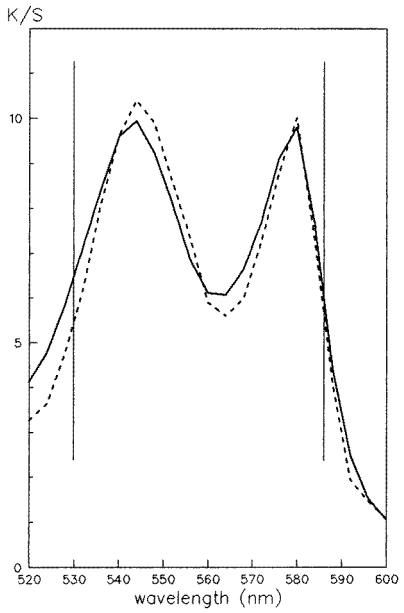

Figure 10. Examples of $K/S_{\mathrm{meas}}(\lambda)$ (full curve) and matched $K/S_{\mathrm{calc}}(\lambda)$ (broken curve). The vertical lines indicate the wavelength range 530–586 nm in which the fitting procedure was performed.

explained by a diminishing role of scattering by small structures having low g values. Our mean result of $g_{\mathrm{fit}} = 0.96$ compares with the result found by Flock *et al* (1987) $g = 0.954$.

Values of g calculated directly from the measured angular intensity functions $h(\theta)$ are about 0.015 higher than those of g_{fit} found by the fitting procedure. This may be ascribed to two effects. Firstly the fitting procedure supplies values of $i(\theta)$ at angles higher than 167° which is the maximum angle at which our equipment can perform measurements. Secondly the measured forwardly scattering peak of $h(\theta)$ is wider than the fitted function $i(\theta)$.

For the connective tissue samples the values found for g_1, b and g_{fit} depend on the thickness of the samples. This indicates that these samples probably already cause multiple scattering, so these values indicate a lower limit of the true values and should not be used further. However, we were unable to prepare thinner, i.e. single-scattering, samples.

5.3. The diffusion constant

The values found for D parallel to the longitudinal direction are significantly higher than those found in the perpendicular direction for the fresh samples. As we expect s to be maximal perpendicular to the longitudinal direction, we expect the measured value of D to be minimal in the case that the longitudinal direction is perpendicular to the inner incident direction. This agrees with the observations.

Table 3 shows that the samples which were frozen and thawed did not show the spatial anisotropy for multiple scattering as observed from the fresh samples. The transmission measurements showed us that spatial anisotropy is not quite lost. But these observations indicate that freezing and thawing have a reasonable effect on the optical scattering properties.

Table 3. Measured values of D mean values ± SEM (mm).

Wavelength (nm)	Orientation of the longitudinal cells with respect to incident direction within the sample	
	Parallel	Perpendicular
Fresh samples		
543.5	0.40 ± 0.05	0.29 ± 0.02
594.1	0.54 ± 0.06	0.47 ± 0.04
632.8	0.66 ± 0.06	0.51 ± 0.07
Frozen and thawed samples		
543.5	0.30 ± 0.03	0.31 ± 0.04
594.1	0.47 ± 0.06	0.45 ± 0.04
632.8	0.51 ± 0.05	0.50 ± 0.03

Assuming a myoglobin concentration of 0.41 mmol l^{-1} and an oxygenation degree of 0.61 we calculated the absorption coefficients a near the three wavelengths. From these values and the values of D we calculated s'_D. With g read from figure 8 we calculated s. These calculations and their results are shown in table 4.

5.4. Spectral reflectance

Diffusion theory and so Kubelka–Munk theory may be applied if $a/s \ll 1 - g^2$ (Furutsu 1980). Within the wavelength range used we can calculate the absorption coefficient as $a \simeq 1.2$ mm^{-1} (3 l $mmol^{-1}$ mm^{-1} × 0.41 mmol l^{-1}); when $s \simeq 14$ mm^{-1} and $g \simeq 0.96$, a/s equals 0.09 and $1 - g^2$ equals 0.08 this is not satisfied. However, lacking simple satisfactory alternatives, we use the ratios K/S although this criterion is not quite satisfied.

5.5. Comparisons

From the collimated transmission measurements of the muscular cell samples we found a mean extinction coefficient of 134 mm^{-1}. This implies a scattering coefficient of about $s_{coll} = 132$ mm^{-1}. From this value and the fitted $g_{fit} = 0.96$ values found from the angular intensity measurements we can estimate the reduced scattering coefficient as $s'_{coll} = s_{coll'}(1 - g_{fit}) = 5.3$ mm^{-1}. This value is much higher than the value found from the reflectance measurements on thick samples $s'_{refl} = 0.85$ mm^{-1}. The difference between s'_{coll} and s'_{refl} can be due to the inaccuracy of the value of g as well as inaccuracy of s_{coll}. The value of $g = 0.993$ needed to match s_{coll} and s_{refl} can be achieved in cases where the differences in refractive index between scatterers and surrounding material is low. In muscular tissue this may be the case, but other investigators, as mentioned in table 1, did not find such high g values for several muscular tissues.

Inaccuracy of s_{coll} may be caused by surface roughness of the samples, because surface refracted light is considered as scattered light. To decrease s_{coll} by a factor of 6, we should collect light on the CCD detector at angles up to 0.4 mrad with respect to the optical axis. A divergence of the unscattered beam of 0.4 mrad can be obtained if small areas of the sample surfaces are tilted with angles up to 8 mrad, which is still very flat. So, this method using a very small angle of acceptance may be very inaccurate. Moreover, we assumed the laser beam to be exactly collimated; this is not the case, its divergence is already 9 mrad, far more than the divergence possibly caused by the surface roughness of the samples.

Table 4. Calculated absorption and scattering coefficients and diffusion constants.

Wavelength (nm)	a_{Omb} (l mmol^{-1} mm^{-1})	a_{Dmb} (l mmol^{-1} mm^{-1})	a[a] (mm^{-1})	D[b] (mm)	s'_D[c] (mm^{-1})	g[d]	s[e] (mm^{-1})
543	3.10	2.37	1.15	0.29	0.745	0.952	15
594	0.61	1.26	0.35	0.47	0.585	0.955	13
632	0.076	0.26	0.061	0.51	0.632	0.958	15

[a] Assuming a myoglobin concentration of 0.41 mmol l^{-1} around 560 nm and an oxygenation degree of 0.61.
[b] Measured, inner incident direction perpendicular to longitudinal direction (see table 3).
[c] $s'_D = 1/3D - 0.35a$.
[d] From figure 8, so perpendicular to the longitudinal direction.
[e] $s = s'_D/(1-g)$.

The value of s'_{refl} has to be considered as a mean value for the whole scattering process, perpendicular as well as parallel to the longitudinal directions. Parallel to the longitudinal direction the scattering coefficient will be lower than perpendicular to this direction. However, we found s'_{refl} values nearly equal to the s'_D values (table 4) which are calculated perpendicular to the longitudinal direction.

Marchesini *et al* (1989) (cf table 1) found a very high value for the scattering coefficient from collimated transmission measurement. We think this value is too high as this agrees with our observations that collimated transmission measurements give results which are too high in s.

Wilson *et al* (1986) found the value of $s' = 0.7$ mm^{-1} (at 633 nm) for ground bovine muscular tissue. Grinding increases the reduced scattering coefficient of chicken breast tissue from 2.7 to 4.5 mm^{-1} (at 633 nm) (Marquez *et al* 1998). If bovine muscular tissue showed the same phenomenon then correction would reduce Wilson *et al*'s result to $s' = 0.42$ mm^{-1}, which two times lower than our value. In view of all uncertainties we consider this agreement as satisfactory.

6. Conclusions

A very small surface roughness and refractive index mismatch between saline and tissue may cause large errors in the values of μ and s' as calculated from collimated transmission measurements.

From angular intensity functions we found $g = 0.96$. The optical diffusion constant D calculated from the oblique incidence measurements depends on the orientation of the sample with respect to the direction of incidence; $D_{\parallel} = 0.66$ mm and $D_{\perp} = 0.51$ mm (at 632 nm). Freezing and thawing of the samples cause a change in the scattering properties, especially if the spatial anisotropy is decreased.

With spectral reflectance measurements, a reduced scattering coefficient of $s' = 0.85$ mm^{-1} around 560 nm and an oxygenation degree of 0.61 are obtained.

Acknowledgments

The authors thank H E Moorlag and N Brouwer for assistance with sample preparation.

References

Antonini E and Brunori M 1971 *Hemoglobin and Myoglobin in Their Reactions with Ligands* (Amsterdam: North-Holland) pp 17–18

Beek J F, Blokland P, Posthumus P, Aalders M, Pickering J W, Sterenborg H J C M and Van Gemert M J C 1997 *In vitro* double-integrating-sphere optical properties of tissues between 630 and 1064 nm *Phys. Med. Biol.* **42** 2255–61

Birth G S, Davis C E and Townsend W E 1978 The scatter coefficient as a measure of pork quality *J. Anim. Sci.* **46** 639–45

Bolin F P, Preuss L E, Taylor R C and Ference R J 1989 Refractive index of some mammalian tissues using a fiber optic cladding method *Appl. Opt.* **28** 2297–303

Davis C E, Birth G S and Townsend W E 1978 Analysis of spectral reflectance for measuring pork quality *J. Anim. Sci.* **46** 634–8

Duntley S Q 1942 The optical properties of diffusing materials *J. Opt. Soc. Am.* **32** 61–70

Flock S T, Wilson B C and Patterson M S 1987 Total attenuation coefficients and scattering phase functions of tissues and phantom materials at 633 nm *Med. Phys.* **14** 835–41

Furutsu K 1980 Diffusion equation derived from space-time transport equation *J. Opt. Soc. Am.* **70** 360–6

Jacques S L, Alter C A and Prahl S A 1987 Angular dependence of HeNe laser light scattering by human dermis *Lasers Life Sci.* **1** 309–33

Judd D B and Wyszecki W G 1963 *Color in Business, Science and Industry* (New York: Wiley)

Lin S-P, Wang L, Jacques S L and Tittel F K 1997 Measurement of tissue optical properties by the use of oblique-incidence optical fiber reflectometry *Appl. Opt.* **36** 136–43

Marchesini R, Bertoni A, Andreola S and Sichirollo A E 1989 Extinction and absorption coefficient and scattering phase functions of human tissues *Appl. Opt.* **28** 2318–24

Marquez G, Wang L V, Lin S-P, Schwartz J A and Thomsen S L 1998 Anisotropy in the absorption and scattering spectra of chicken breast tissue *Appl. Opt.* **37** 798–804

Meador W E and Weaver W R 1979 Diffusion approximation for large absorption in radiative transfer *Appl. Opt.* **18** 1204–8

Molenaar R, ten Bosch J J and Zijp J R 1998 The determination of Kubelka–Munk scattering and absorption coefficients using diffuse illumination (in preparation)

Rhodin J A G 1975 *An Atlas of Histology* (New York: Oxford University Press) pp 128–9

Souci S W, Fachmann W and Kraut H 1969 *Die Zusammensetzung der Lebensmittel* (Stuttgart: Wissenschaftliche)

Wilksch P A, Jacka F and Blake A J 1983 Studies of light propagation through tissue *Porphyrin Localization and Treatment of Tumors* ed D R Doiron and C J Gomer (New York: Liss) pp 149–61

Wilson B C, Patterson M S and Burns D M 1986 Effect of photosensitizer concentration in tissue on the penetration depth of photoactivating light *Lasers Med. Sci.* **1** 235–44